JOURNAL OF MATERIALS SCIENCE **36** (2001) 389–397

Fatigue crack growth analysis of a premium rail steel

H. AGLAN, Y. X. GAN
Mechanical Engineering Department, Tuskegee University, Tuskegee, AL 36088, USA
E-mail: aglanh@acd.tusk.edu

The fatigue crack growth behavior of a premium rail steel was studied using the Modified Crack Layer (MCL) theory. The rate of energy expended on damage formation and evolution within the active zone was evaluated from the hysteresis energy of unnotched and notched specimens. Due to head hardening of the rail, there is a vertical microstructure gradient inside the rail. In this work, the fatigue test specimens were sliced longitudinally from the head of a new rail near the web which represents the microstructure of the base material. The notch length to sample width ratio (a/w) was 0.1. Fatigue tests were performed on both unnotched and single edge notched (SEN) specimens under tension-tension load control condition at 5 Hz. The maximum fatigue stress was 200 MPa, which is about 40% of the yield strength of the material. The minimum to maximum stress ratio was 0.1. The crack length, number of cycles, and hysteresis loops were recorded during the tests from which the crack speed, the energy release rate, and the hysteresis energy for both notched and unnotched specimens were determined. The rate of energy dissipation on damage formation was evaluated based on the difference between the hysteresis energy for the notched and the unnotched specimens. These data were used in the MCL theory to extract the specific energy of damage, γ'; a material parameter characteristic of the fatigue crack growth resistance of the rail steel. It was found that the value of γ' is 1300 kJ/m^3. Three distinctive stages of crack growth kinetics were observed; crack initiation, stable crack growth and unstable crack growth. Microscopic examination of the active zone revealed damage species in the form of microcracks, inter-granular separation, and plastic deformed material. It is these damages that have led to the crack deceleration in the second stage. The fracture surface was also examined. The initiation region showed drawn-out lamellar pearlite. Ductile tearing and coarse ridges with intensive lamellar formation as well as microcracks were observed in the second region. The formation of these damage species has also contributed to the crack deceleration in the second stage of fatigue crack growth kinetics. The unstable crack growth region displayed cleavage facets initiated from the grain boundaries.

1. Introduction

Fracture mechanics has been used to describe the fatigue behavior of metallic materials for a long time and a considerable amount of literature can be found in this field. Stress control and strain control tests have been commonly used to study the fatigue crack propagation behavior. Recently, Soboyejo *et al*. [1] have investigated the fatigue and fracture behavior of a Nb-12Al-44Ti-1.5Mo intermetallic compound. The load-shielding concept as reported by Subramanian, Mendiratta and Dimiduk [2] was applied to describe the crack growth behavior. A relationship between the current stress intensity factor, the initial stress intensity factor and the crack length was established as follows:

$$\frac{K}{K_0} = e^{C(a-a_0)} \tag{1}$$

where, K is the current stress intensity factor, K_0 is the initial stress intensity factor, a is the current crack length, a_0 is the initial notch length, and C is a so called material parameter.

The related fatigue damage mechanisms were also proposed by Soboyejo *et al*. [1]. Accumulation of microplasticity in the form of coarsening of slip bands was the major mechanism in the initiation stage, while unzipping of microcracks along some preferential slip bands contributed to the main crack propagation.

Campbell, Rao and Ritchie [3] studied the fatigue crack growth behavior using γ-Ti Al based intemetallics as candidate materials. In such materials, ligament bridging, crack closure, crack deflection and crack tip shielding ahead of the main crack tip [4, 5] were considered as typical mechanisms which contributed to the increased fatigue fracture resistance. Parameters characterizing the fatigue fracture resistance

of the materials were proposed based on the stress intensity factor concept. The following equation was established to evaluate the effective near tip stress intensity factor:

$$\Delta K_{\text{eff}} = (K_{\max} - K_{\text{br}}) - K_{\text{cl}} \tag{2}$$

where ΔK_{eff} is the effective near tip stress intensity factor, $K_{\max}$ is the maximum stress intensity factor, K_{br} is the bridging stress intensity factor and K_{cl} is the close stress intensity factor.

In the above model, the effect of intrinsic and extrinsic factors on the fatigue fracture resistance was differentiated. Based on experimental determination of the threshold value of the stress intensity factor, the following criteria by which one can determine whether the fatigue crack propagates or not can be proposed.

$$\Delta K_{\text{eff}} \leq \Delta K_{\text{th}} \tag{3}$$

$$\Delta K_{\text{eff}} \geq \Delta K_{\text{th}} \tag{4}$$

If the condition expressed by Equation 3 is met, the crack will be in the state of near threshold and no appreciable growth will occur. If the condition in Equation 4 is satisfied, then the crack will propagate.

In order to correlate the crack speed $\mathrm{d}a/\mathrm{d}N$ with the crack driving force (for example the stress intensity factor range ΔK), the Paris equation has been commonly used [6]. This is expressed as:

$$\frac{\mathrm{d}a}{\mathrm{d}N} = C(\Delta K)^m \tag{5}$$

where C and m are supposed to be material parameters.

In the mid-growth rate regime, the commonly observed linear range of the fatigue crack propagation in brittle materials, the Paris law can closely describe the fatigue kinetics [3], and the exponent m, can be determined experimentally. At both low and high crack speed ranges, nonlinear behavior of $\log(\mathrm{d}a/\mathrm{d}N)$ versus the stress intensity factor range (ΔK), or the energy release rate (J^*) was found [7, 8]. Other fatigue models [9–14] based on the modification of Equation 5 have the same applicability in the near-threshold stage for design purposes.

A strain controlled criteria [15–18] has also been proposed to describe the fatigue crack kinetics. Miner [15] used a simplified Manson-Coffin relationship [17, 18] to describe the fatigue lifetime. In this approach, the contribution of elastic deformation to the fatigue damage was neglected. The fatigue lifetime was thought to be controlled by the plastic strain range. This is expressed as:

$$\Delta\varepsilon_{\text{p}}(N_{\text{f}})^b = C_1 \tag{6}$$

where N_{f} is the cycle to failure, $\Delta\varepsilon_{\text{p}}$ is the plastic strain range. Again, b and C_1 were proposed as material constants. The experimental values of b and C_1 depend on composition, processing conditions, microstructural heterogeneity and the test conditions [19].

Fatigue damage accumulation has also been determined using Palmgren-Miner approach [20, 21]. In this method, the damage is assumed to accumulate in each cycle and failure is considered to occur when the total damage equals unity. The damage at each fatigue cycle was calculated using the following equation.

$$D_{\text{i}} = \left(\frac{1}{N_{\text{f}}}\right)_i \tag{7}$$

where N_{f} is the fatigue lifetime in number of cycles, D_{i} is the damage per cycle. However, experimental tests in stress controlled fatigue demonstrate that effective strain increases in such a way that a cycle applied later results in a greater damage than a cycle applied earlier [22]. This means that the actual damage increases non-linearly which necessitates the modification of the above damage accumulation model of Equation 7.

Chan, Wittkowsky and Pfuff [23] considered the accumulation of fatigue damage under increasing stress condition. The fatigue lifetime, N, under a given stress amplitude, σ, was expressed as:

$$N = \frac{1}{4}\left(\frac{\sigma_{\text{u}} - \sigma_{\text{y}}}{\sigma - \sigma_{\text{y}}}\right)^{\alpha} \tag{8}$$

where σ_{u} is the ultimate tensile strength of the material, σ_{y} is the yield strength of the material and α is assumed to be a material parameter.

If the stress amplitude acting on the specimen increases from σ to σ' after N_0 cycles within the lifetime of the material, the cycles to failure, N', after the stress increase is given by

$$N' = N_0 + \frac{1}{4}\left(1 - \frac{N_0}{N}\right)\left(\frac{\sigma_{\text{u}} - \sigma_{\text{y}}}{\sigma' - \sigma_{\text{y}}}\right)^{\alpha} \tag{9}$$

During fatigue, the link-up of microcracks or secondary cracks is initially very slow, but the rate increases as the number of microcracks and the accumulated fatigue damage increases. The remaining lifetime, N_{r}, which is the difference between N' and N_0 is given by

$$N_{\text{r}} = N' - N_0 = \frac{1}{4}\left(1 - \frac{N_0}{N}\right)\left(\frac{\sigma_{\text{u}} - \sigma_{\text{y}}}{\sigma' - \sigma_{\text{y}}}\right)^{\alpha} \tag{10}$$

The above mechanistic models are based, mainly, on the macro-mechanical behavior of materials.

In the current study, an approach which evaluates the fatigue resistance of materials based on the thermodynamics of irreversible processes and energy expended on damage formation is adopted. This approach has been employed to study the fatigue crack propagation (FCP) behavior of a premium rail steel. The theoretical development as well as the experimental procedures are discussed in the following sections.

2. Theoretical considerations

The modified crack layer (MCL) theory [24] has been developed and employed for the analysis of fatigue crack propagation behavior of various materials including metallic alloys [7, 8], cementitious materials [25–32], adhesively bonded joints [33–36] and polymeric composites [37, 38].

In this theory, the main crack and its surrounding damage are considered as a thermodynamic entity

(active zone). Based on entropy and energy balance considerations, the following equation was formulated.

$$T\dot{S} = (J^* - \gamma' a)\dot{a} + \dot{D} \tag{11}$$

where T is the ambient temperature and $\dot{S}$ is the rate of change of the entropy of the system comprising the crack and the surrounding damage, J^* is the energy release rate, γ' is the specific energy of damage, a material parameter characteristic of its fatigue resistance, a is the crack length, $\dot{a}$ is the crack speed or $\mathrm{d}a/\mathrm{d}N$, N being the number of cycles, $\dot{D}$ is the rate of energy expended on damage formation associated with active zone evolution. At minimum entropy production, the term $T\dot{S} = 0$ and Equation 11 can be written as

$$\frac{\mathrm{d}a}{\mathrm{d}N} = \frac{\dot{D}}{(\gamma' a - J^*)} \tag{12}$$

Under stress control fatigue, the energy release rate J^* can be determined from the change in potential energy as

$$J^* = \frac{1}{B}\left(\frac{\partial P}{\partial a}\right) \tag{13}$$

where P is the potential energy (area above the unloading curve) at each crack length a, and B is the specimen thickness.

The cyclic rate of energy dissipation, $\dot{D}$, associated with active zone evolution was obtained from the difference in the hysteresis energies between the notched and unnotched specimens. The value of $\dot{D}$ can be expressed as:

$$\dot{D} = \frac{1}{B}(H_\mathrm{n} - H_\mathrm{u}) \tag{14}$$

where H_n is the hysteresis energy for the notched specimen at any cycle (N) and H_u is the hysteresis energy for the unnotched specimen at the same number of cycles. A schematic illustration of the procedures to determine the value of the cyclic rate of energy dissipation from fatigue tests on notched and unnotched specimens is shown in Fig. 1.

Rearranging Equation 13 gives:

$$\left(\frac{J^*}{a}\right) = \gamma' - \frac{\dot{D}}{(\mathrm{d}a/\mathrm{d}N)a} \tag{15}$$

The quantities J^*, $\mathrm{d}a/\mathrm{d}N$, $\dot{D}$ and a, are generated from the fatigue crack propagation experiments. If the theory describes the experimental fatigue behavior of the material, the quantities between brackets in Equation 15 should plot as a straight line parallel to the x-axis. The value of the specific energy of damage, γ', is the intercept of the straight line with the y-axis.

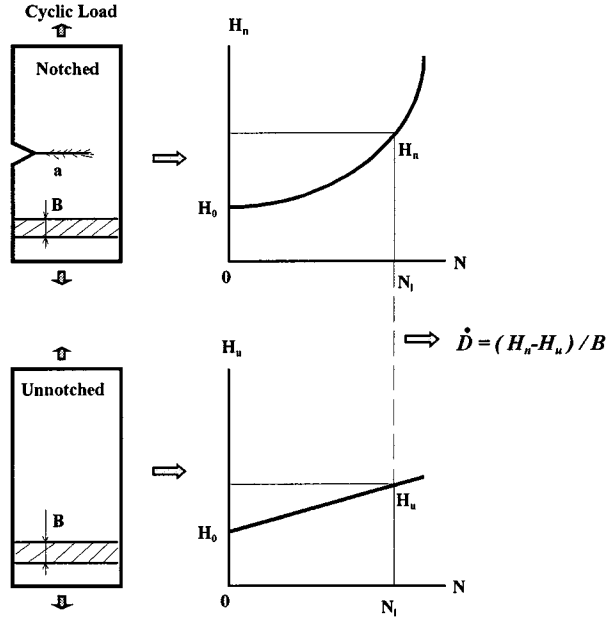

Figure 1 Illustration showing the procedure to evaluate the cyclic rate of energy dissipation, $\dot{D}$.

The calculation of the $\dot{D}$ based on the difference in the hysteresis energies of the notched and unnotched specimens have provided a direct means of accounting for the energy which has been expended on damage formation within the active zone. This has led to the elimination of the energy dissipated into the bulk of material for both notched and unnotched specimens. It should be noted that Equation 15 has only γ' as a material parameter which makes the MCL theory more reliable than other models.

3. Material and experimental procedures

The material used in the present work was a premium rail steel provided by Transportation Technology Center, Inc., Pueblo, Colorado. The chemical composition range of the rail steel is similar to that given in Table I.

The rail head was sliced into thin layers with a thickness of 2.0 mm. Due to head hardening of the rail, there is a vertical microstructure gradient inside the rail. In the present study the middle layer at a depth of about 20 mm from the top of the head was chosen for the fatigue tests. Rectangular specimens with 75 mm length and 18 mm width were machined from that slice. At the center of one free edge of the specimens, a 60° notch was introduced using a very sharp triangle file. The notch depth was about 1.8 mm so that the notch depth to sample width ratio (a/w) was 0.1. Unnotched specimens 75 mm long, 12.5 mm wide and 2 mm thick were prepared for static testing.

Static tensile and fatigue experiments were performed using an 810 materials testing system (MTS)

TABLE I Chemical composition of the premium rail steel

Element	C	Mn	P	S	Si	Ni	Cr	Mo	V
Content % (weight)	0.72∼ 0.78	0.60∼ 1.25	0.035	0.037	0.10∼ 0.60	0.25	0.25∼ 0.50	0.10	0.03∼ 0.05

equipped with a 100 kN load cell. The specimen were gripped between two hydraulic wedge grips. The gage length was 50 mm. Static tests based on unnotched specimens were carried out under displacement control condition. For fatigue tests, both unnotched and notched specimens were used. All the fatigue tests were conducted at ambient temperature of 25 °C under load control conditions using a frequency of 5 Hz. The maximum stress was 200 MPa, and the ratio of minimum stress to maximum stress was 0.1. A sinusoidal wave form of 5 Hz was used. The crack length at various intervals of number of cycles was recorded during the tests. A video camera with a zoom lense was used to view the crack tip region, measure the crack length and capture the damage associated with the crack growth. A total of six samples were tested and data from each sample was used for the fatigue crack propagation analysis and the fatigue damage species examination. These include three identical unnotched samples and three notched samples. In addition, interrupted fatigue crack propagation tests based on three notched specimens were also performed for microscopic examination of the active zone adjacent to the main crack. The side zone was examined using an optical microscope and a Hitachi S-2150 scanning electron microscope, operated at a maximum acceleration voltage of 25 kV. The fracture surface was also examined using the same procedure. Typical micrographs revealing both the damage zone and fracture surface were taken.

4. Results and discussion

4.1. Static behavior

A typical stress-strain curve of the rail steel specimen taken from the middle section of the rail head is shown in Fig. 2. It displays elastic behavior followed by nonlinear plastic behavior. The stress was calculated based on the original cross-sectional area before testing. In the strain range up to 0.25%, the relationship between stress and strain is linear. The calculated Young's modulus is about 200 GPa. In the strain range from 1% to 9%, the stress-strain relationship is highly nonlinear. The material reached its ultimate strength of 1100 MPa. This relationship was used to select the maximum and minimum stresses for the fatigue tests. The maximum fatigue stress was 200 MPa which is about 40% of the yield stress, depicted in Fig. 2.

4.2. Fatigue crack growth parameters

4.2.1. Fatigue lifetime and crack speed

A plot of the crack length, a, versus the number of cycles, N, for the premium rail steel is shown in Fig. 3. It can be seen from Fig. 3 that the total fatigue lifetime of the steel is approximately 70,000 cycles. The initiation lifetime was about 20,000 cycles and the propagation lifetime is about 50,000 cycles. The crack length grew up to about 10.0 mm after initiation. The crack propagated very fast in the last several hundred cycles, and the critical crack length reached about 12 mm. The slope of the curve in Fig. 3 is taken as the average crack speed at each crack length. The relationship between the crack speed, da/dN, and crack length, a, is shown in Fig. 4. The curve shown in this figure demonstrates a crack growth kinetics of a sigmoidal feature, which can be

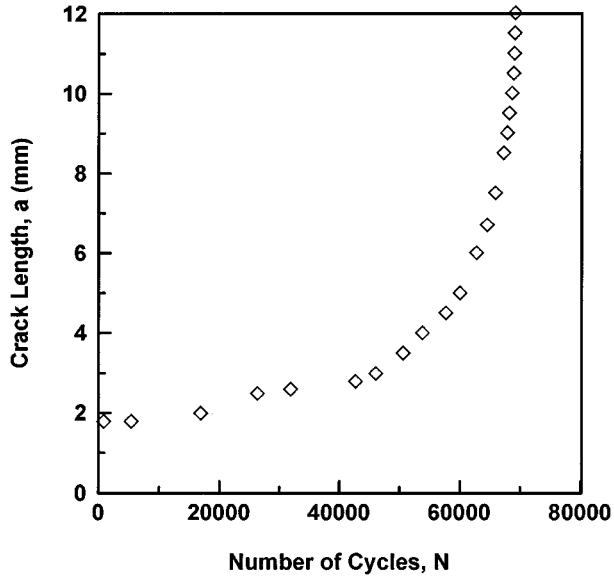

Figure 3 Fatigue crack length, a, versus the number of cycles N.

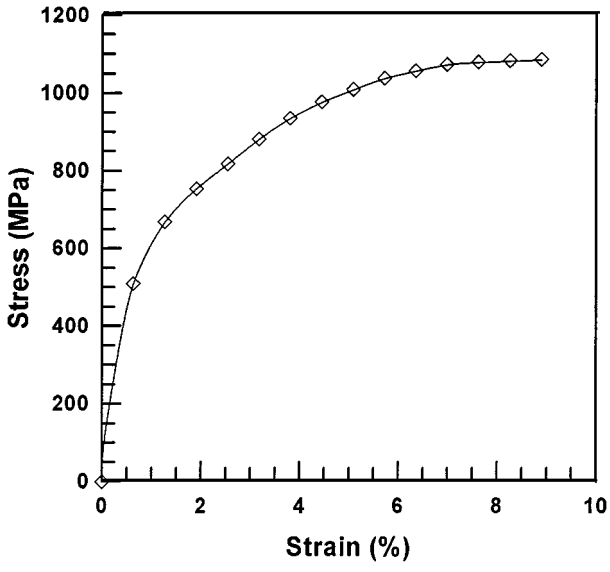

Figure 2 Stress-strain relationship of the premium rail steel.

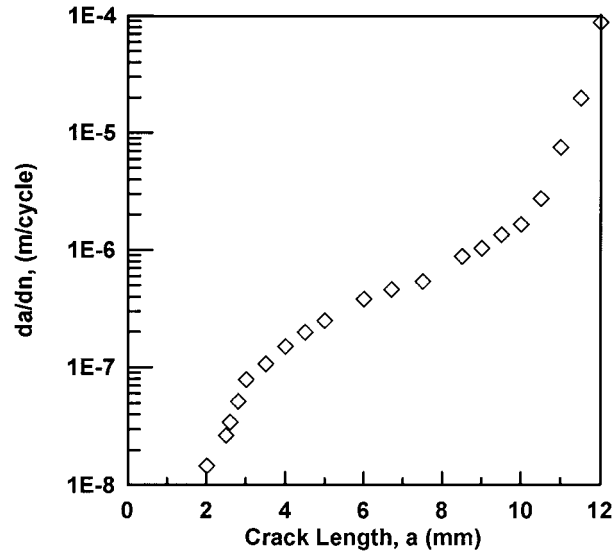

Figure 4 Fatigue crack speed, da/dN, versus crack length, a.

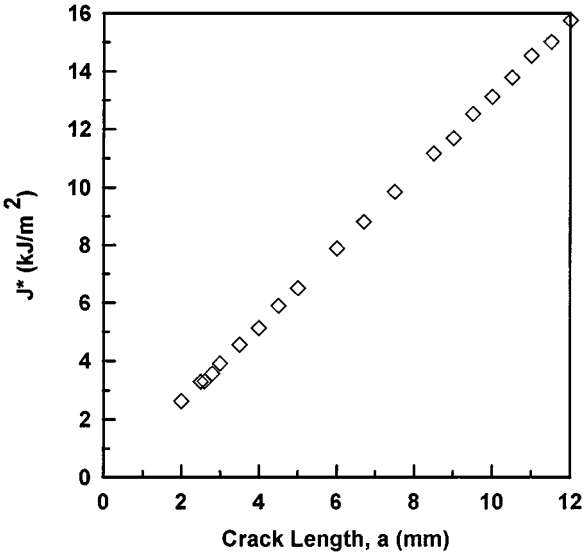

Figure 5 Energy release rate, J^*, versus the fatigue crack length, a.

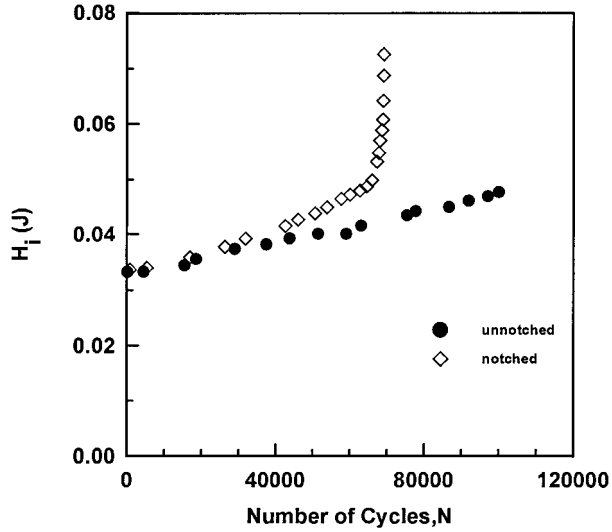

Figure 6 Hysteresis energy for both notched and unnotched specimens versus the number of cycles.

divided into three distinct stages. The first stage is the crack initiation or the threshold. In the second stage, a crack deceleration is observed. It is due to the damage formation and evolution in the vicinity of the main crack, which will be discussed in more detail later. The curve approached asymptotic values in the third stage (critical stage). In all the three stages, the crack growth rate varied appreciably.

4.2.2. The energy release rate

The potential energy, P, was calculated from the hysteresis loops recorded at intervals of number of cycles. It is the area above the unloading curve at each crack length. On this basis, the relationship between the potential energy and the fatigue crack length, a, was established. The relationship between the potential energy and the crack length was used to determine the energy release rate using Equation 13. Fig. 5 illustrates the energy release rate, J^*, as a function of the crack length, a, for a typical rail steel specimen. This relationship between J^* and, a, displayed in Fig. 5 will be used in the MCL theory to determine the value of the specific energy of damage, γ'.

4.2.3. The hysteresis or damage energy

The hysteresis energies for the notched and unnotched specimens, H_n and H_u respectively, were calculated from the area of hysteresis loops recorded during the fatigue experiments at intervals of number of cycles. The hysteresis area was measured, using a planimeter, from the hysteresis loops. The hysteresis energy corresponding to each cycle was then calculated. The value of, H_n, includes the energy expended on damage processes associated with crack growth and energy dissipated into the bulk of the material for the notched specimens. The hysteresis energy calculated based on the unnotched specimens, H_u, comprises only the energy dissipated into the bulk of the material. Both H_n and H_u are irreversible energies. The relationship between hysteresis energy and the number of cycles, N, for both notched specimens and unnotched specimens is shown in Fig. 6. The value of H_n for a notched specimen is higher than that for an unnotched specimen, since it contains the portion of the irreversible energy expended on damage formation within the active zone. The relationship between H_u and N is almost linear, while for the notched specimen, the hysteresis energy, H_n, increases remarkably with the increase in the number of cycles or the crack length a.

The cyclic rate of energy dissipation into active zone evolution, $\dot{D}$, which is given by Equation 14 can be determined from Fig. 6. The relationship between $\dot{D}$ and the crack length, a, for the premium rail steel is shown in Fig. 7. Two regions can be found in Fig. 7. In the crack initiation stage, corresponding to the crack length from the initial 1.8 mm to about 3.0 mm, the value of $\dot{D}$ is very small; less than 2.0 (J/m·cycle). In the crack propagation region, which corresponds to the crack length range from 3 mm up to approximately 10 mm, there is a large change in the value of $\dot{D}$. This is the energy expended on damage formation within

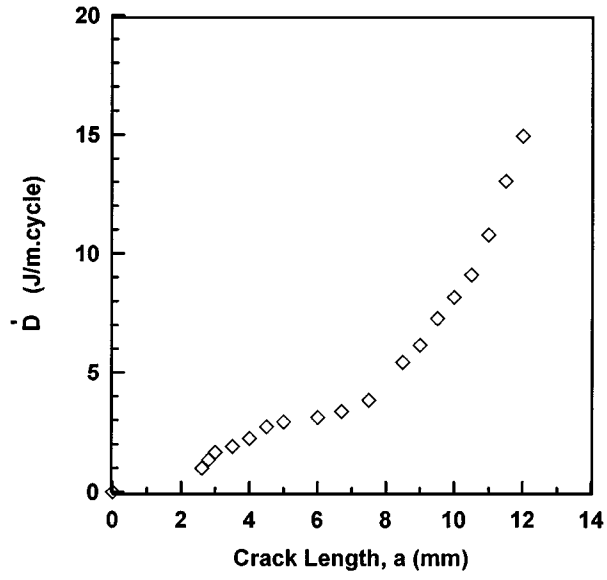

Figure 7 Cyclic rate of energy dissipation, $\dot{D}$, versus the fatigue crack length, a.

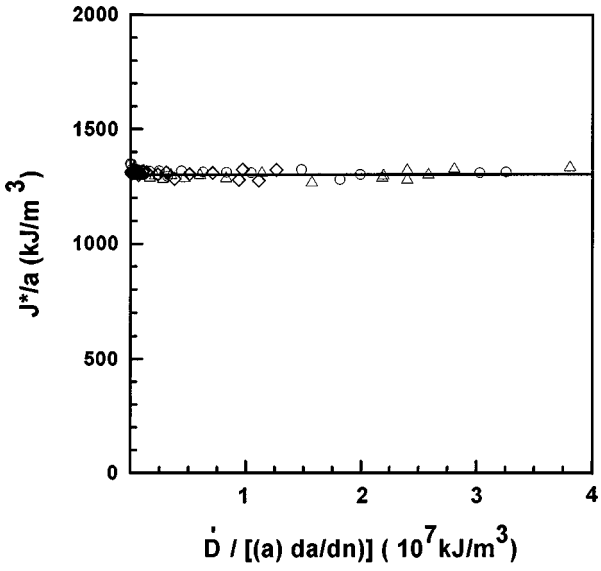

Figure 8 Fatigue crack propagation data for obtaining γ' using the Modified Crack Layer (MCL) theory.

the active zone. The increase of $\dot{D}$ with crack length in this stage should be much faster than that of $\dot{D}$ in the first stage (crack initiation stage). Thus, the rail steel dissipated an appreciable amount of energy during the fatigue crack growth. This in turn has reduced the crack driving force and resulted in the deceleration of the main crack.

4.2.4. Specific energy of damage, γ'

The parameters γ' was evaluated using the MCL theory along with the experimental parameters previously calculated: a, $\mathrm{d}a/\mathrm{d}N$, J^*, and $\dot{D}$. The relationship between J^*/a and $\dot{D}/[a(\mathrm{d}a/\mathrm{d}N)]$ for the rail steel specimens is shown in Fig. 8. If the experimental results are in accord with the MCL model, of Equation 15, a plot of J^*/a versus $\dot{D}/[a(\mathrm{d}a/\mathrm{d}N)]$ should give a straight line parallel to the x-axis. Indeed, based on the results presented in Fig. 8, a straight line which is parallel to the horizontal axis is obtained. The value of, γ', is the intercept of the line with the y-axis. This attests to the applicability of the MCL model to describe the FCP behavior of the rail steel. The specific energy of damage, γ', is considered as a material property and has a value of about 1300 kJ/m^3, for the rail steel under consideration. This value is less than that of some vanadium alloys [7]. A larger value of γ' indicates higher resistance to FCP since more energy is required to cause a unit volume of the material to change from an undamaged state to a damaged state.

From the above analysis, it can be seen that γ' is independent of the different stages of the crack growth kinetics. Although $\dot{D}$ contains the information of the energy dissipated into the active zone formation, it has an intensive dependency on the fatigue crack growth kinetics. A consistent value of $\dot{D}$ cannot be obtained over the entire energy release rate range for the same material. This indicates that $\dot{D}$ is not as significant as γ' to characterize the fatigue crack growth resistance of the material. The rationale of the consistency of γ' in different stages of fatigue crack growth kinetics can be explained as follows.

It can be seen from the fatigue crack propagation (FCP) data as shown in Fig. 5, that the energy release rate, J^*, increases as the crack propagates. In the entire energy release rate range, the change of the left term J^*/a in the MCL model as shown in Equation 15 can be leveled by both the increasing of J^* and the crack length, a. The variation of the term in the right side of Equation 15, $\dot{D}/[a(\mathrm{d}a/\mathrm{d}N)]$, depends on several factors. These are the crack length, a, the crack speed, $\mathrm{d}a/\mathrm{d}N$ and $\dot{D}$, the irreversible energy dissipated into the damage formation in the active zone. On one hand, it is clear that the crack speed changes with the crack length and this trend is clear in Fig. 4. The larger the crack length, the higher the crack speed. On the other hand, there exists some relationship between $\dot{D}$ and crack length, a. Experimental results show that the value of $\dot{D}$ increases with the increase in the crack length, a, as show in Fig. 7. Thus, the variation of $\dot{D}$ can be well balanced by the change in both a and $\mathrm{d}a/\mathrm{d}N$. If $\dot{D}$ has a higher value, it corresponds to a larger crack length and a higher crack speed. A higher value of $\dot{D}$ indicates an increase in the energy dissipated into the active zone of the material, which means more energy was absorbed by the specimen for the damage transformation. Thus, an increasing $\dot{D}$ would result in an increase of both a and $\mathrm{d}a/\mathrm{d}N$. This would keep the term $\dot{D}/[a(\mathrm{d}a/\mathrm{d}N)]$ from changing much. Instead, it varies harmoniously with the left term, J^*/a, in Equation 15 so that the linear relationship between J^*/a and $\dot{D}/[a(\mathrm{d}a/\mathrm{d}N)]$ is maintained over the entire crack driving force or energy release range. Thus, a consistent value of γ', 1300 k J/m^3 can be obtained, though the crack growth kinetics change from one stage to another. The independency of γ' on fatigue crack growth speed and fatigue crack length demonstrated the validity of the MCL theory in describing the fatigue behavior of the premium rail steel and the rationale of using γ' as the sole parameter characteristic of the fatigue crack grow resistance of the material.

The crack speed versus the energy release rate for the rail steel is shown in Fig. 9. It can be seen from Fig. 9

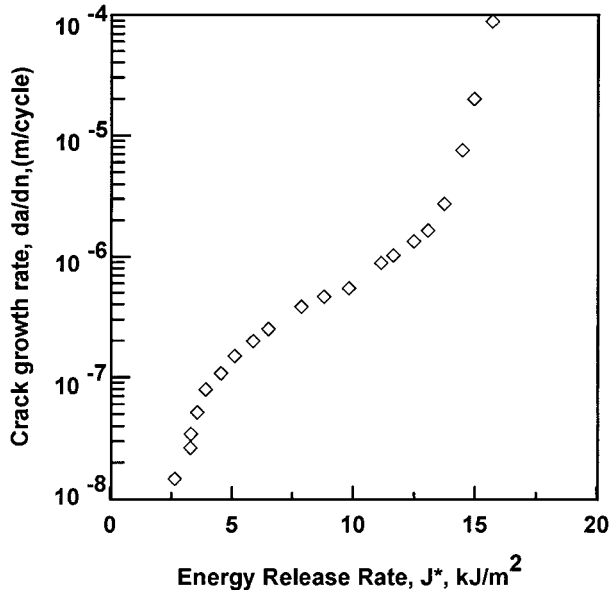

Figure 9 Fatigue crack speed versus the energy release rate.

that the curve displays an S-shaped behavior, indicating three stages of FCP kinetics. A threshold stage is followed by a stage of decreased acceleration and then a stage of unstable crack propagation. This analysis of the fatigue crack propagation kinetics is basically in agreement with the calculated results of crack speed, da/dN, versus crack length, a as shown in Fig. 4. The decreased acceleration in the crack speed is indicative of material damage ahead of the crack tip. The current fatigue analysis is different from those based on the Paris law, in which the relationship between $\log(da/dN)$ and ΔK is assumed to be linear, as reported by Stone *et al*. [39–41] for several types of rail steel. In the slow crack growth rate range of near threshold, the Paris Law generally gives an engineering approximation for the prediction of the fatigue crack speed. The current approach focuses more on the crack propagation behavior which is very common in the rails with detectable defects such as detail cracks or pipings. In the following section, a fatigue damage evaluation will be presented based on the morphological examination of the fatigue fracture surface and the side zone (active zone).

4.3. Morphological analysis of fatigue damage in rail steel

4.3.1. Fatigue fracture surface morphology

A schematic representation of the fatigue fracture surface with various regions for a typical rail steel specimen is shown in Fig. 10. The notch is at the left hand side of the figure. The fatigue crack propagation direction is from left to right. The fracture surface can be divided into three distinct regions according to the morphological features. Region I is the crack initiation. Region II is the stable crack propagation, and Region III is the fast crack propagation. These three regions are related to the three stages of fatigue fracture kinetics, crack initiation, stable crack propagation and fast crack growth, as previously discussed.

The first region is about 1.2 mm in length and contains the fatigue damage species associated with the near threshold crack propagation. At a magnification of 1000×, pulled-up pearlite lamella, limited microcracks and micro-voids can be found in Fig. 11, a micrograph taken from location "A" as shown in Fig. 10. These features indicate a ductile fracture mechanism related to the first stage of crack growth.

The second region is the stable crack propagation region which is about 7 mm in length. This region is characterized by inter-granular separation, tearing ridges

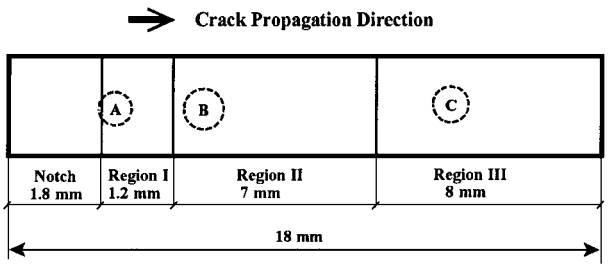

Figure 10 Schematic representation of the fatigue fracture surface showing the fatigue regions and location of micrographs for fatigue damage analysis.

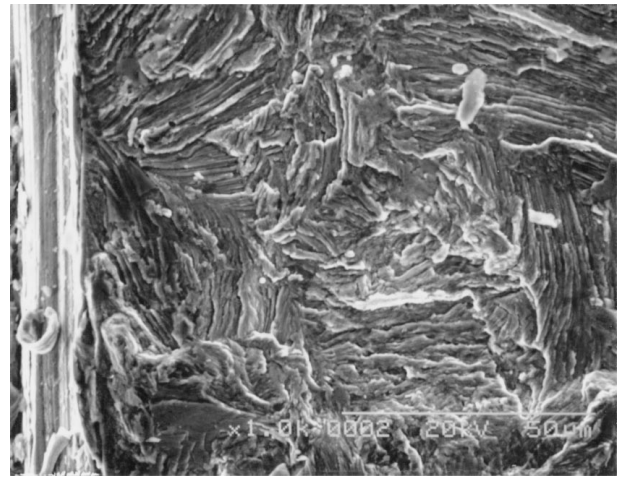

Figure 11 SEM micrograph at 1000× of the first region, showing pull-up pearlite, lamella, limited microcracks and microvoids.

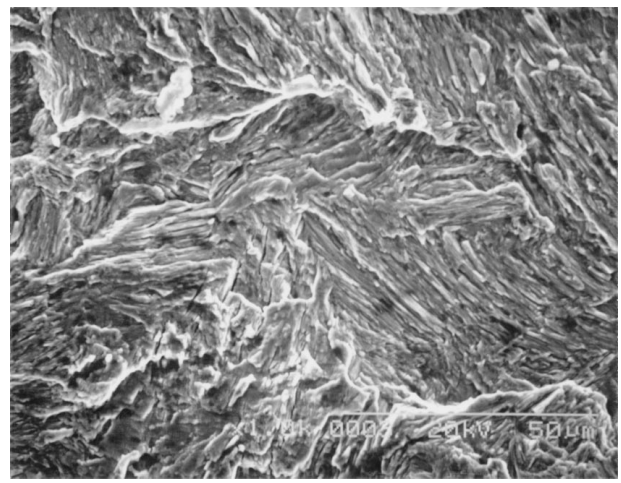

Figure 12 SEM micrograph at 1000× of the second region, showing the intergranular separation, tearing ridges and microcracks.

and microcracks. Such features can be found in Fig. 12, a 1000× micrograph taken from location "B" as shown in Fig. 10. These features reflect the crack deceleration and indicate that a considerably high energy consuming process is associated with crack propagation.

The third region is the unstable crack propagation region which is about 8 mm in length. This region is characterized by fast crack propagation features. Cleavage and intergranular separation were observed. Fig. 13, a micrograph taken from location "C" in Fig. 10, illustrates typical features of this region. Cleavage facets originated from grain boundaries are readily found. In some areas, there exist intergranular cracks and voids along the grain boundaries as shown in the left hand section and the middle part of the micrograph in Fig. 13.

4.3.2. Morphology of the active zone

Interrupted fatigue tests were performed for active zone examination. The fatigue crack was controlled to grow up to 8 mm, and then the test was interrupted. The specimen was taken away from the MTS machine for both optical and SEM examinations. Analysis of the active zone can provide direct micro-mechanics evidence for the determination of the fatigue damage of the material.

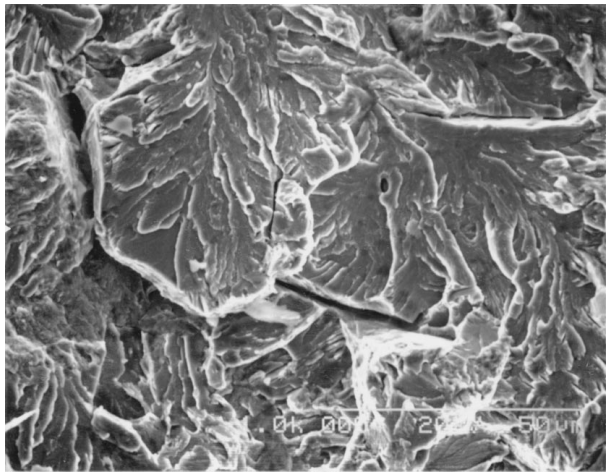

Figure 13 SEM micrograph at 1000× of the third region, showing cleavage and intergranular separation.

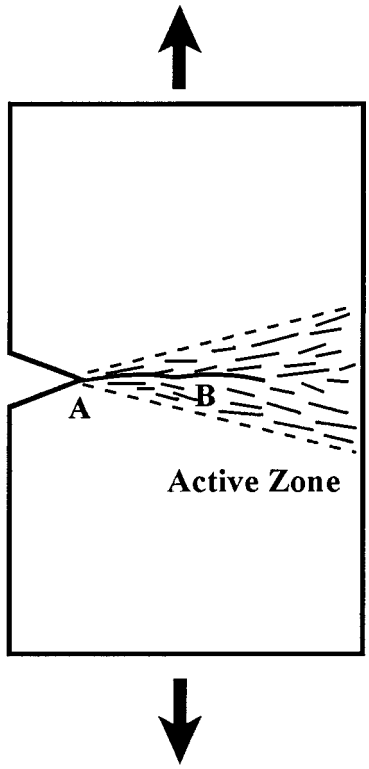

Figure 14 Schematic representation of the side view of the fatigue specimen showing the active zone and the location of micrographs for the side damage analysis.

The active zone, as schematically shown in Fig. 14, precedes the crack tip and it evolves during the main crack growth. The active zone evolution is an irreversible process. Fracture can be envisioned as "the motion" of the active zone. From the micro-mechanics view, the extent of damage during the crack propagation determines the fatigue associated energy conversion mechanism and it should be considered in the evaluation of the resistance of a material to FCP. For the rail steel used in this study, the active zone was examined at different crack lengths.

In the first region (fatigue crack initiation stage) the active zone is characterized by shear deformation, plastic flow and microcracks in the vicinity of the main crack. An SEM micrograph at 2000×, taken from location "A" in Fig. 14, displays the crack initiation stage

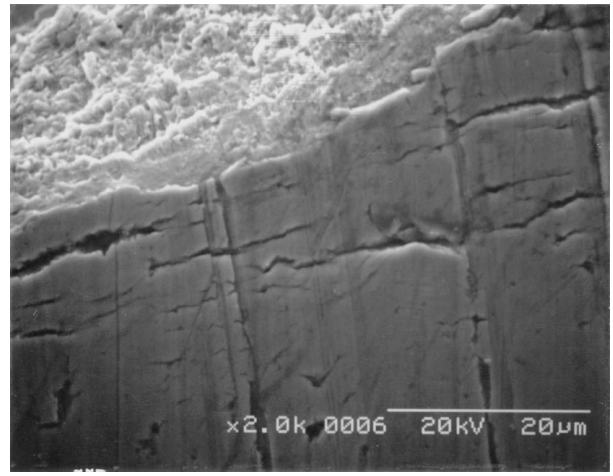

Figure 15 SEM micrograph at 2000× of the active zone in the first region, showing damage species in the form of shear deformation, plastic flow and microcracks.

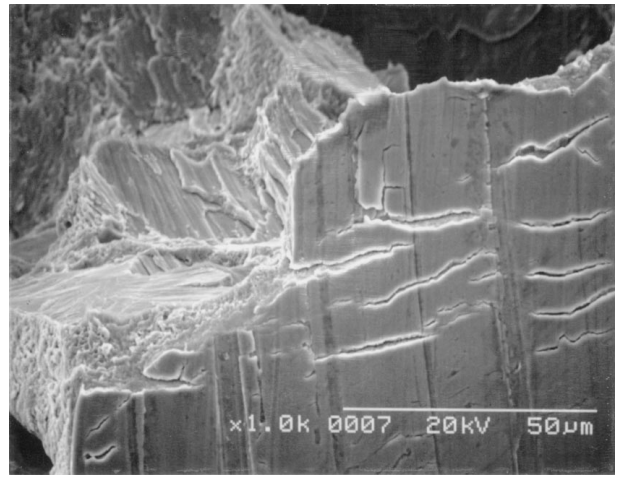

Figure 16 SEM micrograph at 1000× of the active in the second region, showing microcracks, and severely damaged material near the main crack.

features as given in Fig. 15. Microcracks and discontinuity of the materials within the active zone can be seen in the middle section of Fig. 15. An SEM micrograph, Fig. 16, taken at 1000× from location "B" in Fig. 14, displays many microcracks, and severely damaged material near the main crack. The orientation of these microcracks is parallel to the main crack. The formation of such feature is due to the accumulation of damage under repeated loading. The higher the density of the microcrack, the more energy is dissipated into the active zone for transforming the material from undamaged state to damaged state. This again can explain the fatigue crack deceleration in the second stage of the FCP kinetics.

5. Concluding remarks

The fatigue crack growth behavior of premium rail steel was studied based on the MCL theory. The following conclusions can be drawn:

1. The modified crack layer theory is applicable for describing the fatigue crack propagation behavior of the rail steel. The specific energy of damage (γ'), characteristic of the fatigue fracture resistance of the

base rail steel under consideration was found to be 1300 kJ/m^3.

2. Severe damage formation in the form of micro-discontinuity, shear-deformed material and micro-cracks was observed within the active zone of the rail steel.

3. The fracture surface morphology shows drawn-out pearlite lamella indicating the ductile failure mechanism in the threshold or initiation stage. The stable crack growth region displays intensive tearing ridges and microcracks indicative of a high energy dissipation process. The unstable crack growth region displays cleavage with inter-granular separation.

Acknowledgments

This work was supported by the Federal Railway Administration, US Department of Transportation (DOT). The guidance and support of the FRA technical monitor, Mr. M. Fateh is greatly appreciated. The authors acknowledge the support of Mr. Gunars Spons, resident engineering manager, Transportation Test Center, USDOT, Pueblo CO. The useful discussion and suggestions provided by scientists and engineers from the TTCI, Pueblo, CO, is also appreciated.

References

1. W. O. SOBOYEJO, J. DIPASQUALE, F. YE, C. MERCER, T. S. SRIVATSAN and D. G. KONITZER, *Metall. Mater. Trans.* **30A** (1999) 1025.
2. P. R. SUBRAMANIAN, M. G. MENDIRATTA and D. M. DIMIDUK, *J. Met.* **48** (1996) 33.
3. J. P. CAMPBELL, K. T. RAO and R. O. RITCHIE, *Metall. Mater. Trans.* **30A** (1999) 563.
4. A. G. EVANS, *J. Am. Ceram. Soc.* **73** (1990) 15.
5. R. O. RITCHIE, *Mater. Sci. Eng.* **A103** (1998) 15.
6. P. C. PARIS and F. ERDOGAN, *J. Basic Eng.* **85** (1963) 528.
7. H. AGLAN, Y. X. GAN, B. CHIN and M. GROSSBECK, *J. Nucl. Mater.* **237** (1999) 192.
8. *Idem., ibid.* **278** (2000) 186.
9. R. G. FORMAN, V. E. KEARNEY and R. M. ENGLE. *J. Basic Eng.* **89** (1967) 459.
10. S. PEARSON, *Eng. Fract. Mech.* **4** (1972) 9.
11. B. MUKHERGEO and D. J. BURNS, *J. Exp. Mech.* **11** (1971) 433.
12. S. ARAD, J. C. RADON and L. E. CULVER, *J. Mech. Eng. Sci.* **13** (1971) 75.
13. J. C. RADON, S. ARAD and L. E. CULVER, *Eng. Fract. Mech*, **6** (1974) 195.
14. C. A. M. BRANCO, J. C. RADON and L. E. CULVER, *J. Test Eval.* **3** (1975) 195.
15. M. A. MINER, *J. Appl. Mech.* **12** (1945) A159.
16. O. H. BASQUIN, in Proceedings, American Society for Testings and Materials, West Conshohocken, PA, (1910) Vol. 10, p. 625.
17. S. S. MANSON, in Proceedings, Heat Transfer Symposium, University of Michigan Engineering Research Institute, 1953, p. 69.
18. L. F. COFFIN, *Transactions, American Society of Mechanical Engineers* **76** (1954) 931.
19. V. KLIMAN, P. FULEKY and J. JELEMENSKA, Advances in Fatigue Lifetime Predictive Techniques (3rd Conference), ASTM STP 1292 (American Society for Testing and Materials, West Conshohocken, PA, 1996) p. 305.
20. H. O. FUCHS and R. I. STEPHENS, "Metal Fatigue in Engineering" (John Wiley and Sons, New York, NY, 1980) p. 67.
21. J. A. BANNANTINE, J. J. COMER and J. H. HANDROCK, "Fundamentals of Metal Fatigue Analysis" (Pretice Hall, Englewood Cliffs, NJ, 1990) p. 188.
22. S. W. TIPTON, in Advances in Fatigue Lifetime Predictive Techniques (3rd Conference), ASTM STP 1292 (American Society for Testing and Materials, West Conshohocken, PA, 1996) p. 283.
23. K. S. CHAN, B. WITTKOWSKY and M. PFUFF, *Metall. Mater. Trans.* **30A** (1999) 1023.
24. H. AGLAN, *Int. J. Damage Mech.* **2** (1993) 53.
25. H. AGLAN, I. SHEHATA, L. FIGUEROA and A. OTHMAN, Trans. Research Record 1353, TRB, Wash., D.C., 1992, p. 24.
26. H. AGLAN and J. L. FIGUEROA, *J. of Eng. Mech.* **119** (1993) 1243.
27. H. AGLAN, *J. of Elas. and Plas.* **25** (1993) 307.
28. H. AGLAN, A. OTHMAN, L. FIGUEROA and R. ROLLINGS, Trans. Research Record 1417, TRB, Wash., D.C., 1993, p. 178.
29. H. AGLAN, A. OTHMAN and L. FIGUEROA, Trans. Research Record 1449, TRB, Wash., D.C., 1994, p. 57.
30. *Idem., J. Mater. Sci.* **29** (1994) 4786.
31. A. OTHMAN, L. FIGUEROA and H. AGLAN, Trans. Research Record 1492, TRB, Wash., D.C., 1995, p. 129.
32. H. AGLAN and F. M. BAYOMY, Trans. Research Record 1568, TRB, Wash., D.C., 1997, p. 17.
33. H. AGLAN, Z. ABDO and S. SHROFF, *J. of Adhs. Sci. and Tech.* **9** (1995) 177.
34. Z. ABDO and H. AGLAN, *J. of Mater. Sci. Lett.* **15** (1996) 469.
35. *Idem., J. of Adhs. Sci. and Tech.* **11** (1997) 941.
36. H. AGLAN and Z. ABDO, *ibid.* **10** (1996) 183.
37. Z. ZHANG, H. AGLAN, P. FAUGHNAN and C. BRYAN, *J. Reinforced Plastics and Comp.* **17** (1998) 752.
38. H. AGLAN, Y. GAN, M. EL-HADIK, P. FAUGHNAN and C. BRYAN, *J. Mater. Sci.* **34** (1999) 83.
39. D. H. STONE, *Canadian Metallurgical Quarterly* **21** (1982) 17.
40. G. T. GRAY III, A. W. THOMPSON, J. C. WILLIAMS and D. H. STONE, *ibid.* **21** (1982) 73.
41. D. H. STONE, S. MARICH and C. M. RIMNAC, Transportation Research Record 744, (1980) p. 16.

Received 24 November 1999
and accepted 22 June 2000